Aqueous nickel(II) hydroxycarbonate instead of nickel(0) colloids as precursors of stable Ni-silica based catalysts for the dry reforming of methane

Oscar Daoura, Ghenwa El Chawich, Maya Boutros, Nissrine El Hassan, Pascale Massiani, Ovidiu Ersen, Walid Baaziz, Franck Launay

Aqueous nickel(II) hydroxycarbonate instead of nickel(0) colloids as precursors of stable Ni-silica based catalysts for the dry reforming of methane

Oscar Daoura[a,b], Ghenwa El Chawich[a,b], Maya Boutros[a], Nissrine El Hassan[c], Pascale Massiani[b], Ovidiu Ersen[d], Walid Baaziz[d], Franck Launay[b*]

[a] Université Libanaise, Laboratoire de Chimie Physique des Matériaux (LCPM/PR2N), Faculté des Sciences II, Campus Fanar, BP 90696 Jdeideh, Lebanon

[b] Sorbonne Université, CNRS, Laboratoire de Réactivité de Surface, LRS, Campus Pierre et Marie Curie, F-75005 Paris, France.

[c] University of Balamand, Faculty of Engineering, Department of Chemical Engineering, P.O. box 33, Amioun El Koura, Lebanon.

[d] Institut de Physique et de Chimie des Matériaux de Strasbourg (IPCMS), UMR 7504 CNRS - Université de Strasbourg, 23 rue de Loess, BP43, 67034 Strasbourg Cedex 2, France.

Corresponding author: franck.launay@sorbonne-universite.fr

Abstract:

Nickel(II) hydroxycarbonate colloids were synthesized in water by the reaction of nickel(II) with carbonate in the presence of hexadecyltrimethylammonium bromide. Then, they were dispersed onto SBA-15 affording, after calcination and reduction, a supported 3 wt.% nickel(0) catalyst for the dry reforming of methane (DRM). This material, compared to reference ones obtained by impregnation, either by organic Ni(0) colloids or by aqueous nickel(II), was characterized by small nickel nanoparticles leading to improved activity and stability. Such use of aqueous nickel(II) hydroxycarbonate colloids instead of organic Ni(0) ones synthesized with harmful reagents is a new and a more efficient and environment-friendly approach.

KEYWORDS:

Aqueous colloids; Greener synthesis; Dry reforming of methane; Nickel hydroxycarbonates

1. Introduction

Supported nickel(0) nanoparticles are widely used as catalysts for the Dry Reforming of Methane (DRM) [1-8] which allows the conversion of two greenhouse gases, *i.e.* CH_4 and CO_2, into hydrogen enriched syngas (H_2:CO) suitable for the production of useful products such as hydrocarbons *via* the Fischer-Tropsch synthesis [9-10] (Eq. 1). In particular, DRM is well-adapted for the valorization of feedstocks with high levels of CO_2 and CH_4 such as biogas.

$$CH_4 + CO_2 \rightarrow 2\ CO + 2\ H_2 \qquad \text{(Eq. 1)}$$

The Ni-based heterogeneous catalysts are usually prepared by the impregnation of supports with aqueous nickel (II) salts followed by drying and calcination steps resulting in supported NiO species that are further reduced *in-situ* before their use in DRM. However, metallic nickel suffers from sintering and coke deposition due to the harsh experimental conditions needed (T ~ 600-800°C) for DRM and the solid carbon generated by side reactions such as by methane decomposition [11]. In some approaches, the use of supports with high specific surface areas and finely controlled pore volumes able to confine small Ni nanoparticles resulting in high dispersion, is considered to be a good strategy to enhance the stability of Ni-based catalysts [12]. However, methods that lead to total nickel confinement and good dispersion are either not straightforward or may increase the cost of the preparation process, which is not favorable to industrial applications. Controlling the size of nanoparticles and, especially Ni ones, before their deposition onto supports using a colloidal approach, could enhance their dispersion given that strong interactions exist between these particles and the support in order to withstand treatments at high temperatures [13-16].

A well-known protocol for the synthesis of stable nickel colloids with adjustable particle sizes consists in the reduction of the metal salt in the presence of trioctylphosphine and oleylamine (considered as hazardous), used as reducing and stabilizing agents, in the absence of any solvent [13]. However, both compounds lead to a very viscous suspension which is not prone to afford a homogeneous dispersion of the particles throughout the porosity of the support during the impregnation step. Moreover, the latter should be carried out at relatively high temperature. Unfortunately, unlike the noble metals for which it is possible to obtain aqueous

suspensions stabilized in particular by hydrophilic quaternary ammonium salts, such as hexadecyltrimethylammonium halides [17-18], stable nickel(0) nanoparticles suspended in water are not easily obtained. Indeed, Ni(0) tends to be readily oxidized and returns quickly to the starting salt. Instead of using pre-formed organic nickel(0) colloids, we propose here an original strategy relying on the use of aqueous nickel(II) hydroxycarbonate colloids prepared by the reaction of Ni(II) ions with ammonium carbonate in the presence of hexadecyltrimethylammonium bromide (HEA16Br used as stabilizing agent). Our approach is doubly interesting. First, the viscous organic media of Ni(0) colloids is replaced by water, and secondly, the hydroxycarbonate particles should have a better affinity with silica than Ni(0) colloids during the thermal treatment needed for the calcination of HEABr and the conversion of Ni hydroxycarbonate into NiO under air then Ni(0) under H_2.

2. Experimental

2.1 Preparation of Ni-based catalysts from colloids

2.1.1 Aqueous suspension of nickel(II) hydroxycarbonate

Nickel nitrate ($Ni(NO_3)_2.6H_2O$, 0.38 mmol) was dissolved in 5 mL of water. In parallel, hexadecyltrimethyl ammonium bromide (HEA16Br, 0.72 mmol) and ammonium carbonate ($(NH_4)_2CO_3$, 0.95 mmol) were dissolved in 95 mL of water, then added to the first solution. The obtained suspension with slightly green color was named $Ni^{II}_{aq.coll}$.

Hexadecyltrimethyl ammonium bromide was synthesized according to the procedure described by Cerichelli et al [19].

2.1.2 Organic suspensions of nickel(0)

The syntheses of Ni(0) colloids in organic medium, $Ni_{org.coll(2)}$ and $Ni_{org.coll(5)}$, with 2 nm and 5 nm average diameter were carried out using the protocols described by Woo Han et al [13] (see details in Supp. information section).

2.1.3 Deposition of the pre-formed colloids and calcination

An appropriate amount of SBA-15 silica (S) [20] was added to the organic or aqueous colloidal suspensions (1 g of SBA-15 for $Ni^0_{org.coll(2)}$/S, 0.7 g for $Ni^0_{org.coll(5)}$ /S at 70°C or 0.4 g for $Ni^{II}_{aq.coll}$ at RT) to get a final material with 5 wt.% of Ni. Then, the resulting mixture was stirred for 24 h. The $Ni^0_{org.coll(2)}$/S, $Ni^0_{org.coll(5)}$/S and $Ni^{II}_{aq.coll}$/S materials were obtained after filtration, washing of the solid with ethanol (case of "organic" colloids) or water (case of aqueous colloids) and drying at 50°C. Two other samples, $Ni^0_{org.coll(2)}$/MCF and $Ni^0_{org.coll(5)}$/MCF, were prepared using MCF silica [12] instead of SBA-15. All those impregnated materials were calcined under air at 550°C during 2 h in order to get NiO-based solids ($Ni^{II}_{aq.coll}$/S, $Ni^{II}_{org.coll(2)}$/S, $Ni^{II}_{org.coll(5)}$/S, $Ni^{II}_{org.coll(2)}$/MCF and $Ni^{II}_{org.coll(5)}$/MCF).

2.2 Catalysis tests

The different materials were tested with a PID ENG & TECH Microactivity Effi Reactor. 50 mg of powdered calcined material were loaded into the reactor (on quartz wool) and reduced *in-situ* at 650 °C for 2 h (10 °C min^{-1}) in a 5% H_2/Ar flow (30 mL min^{-1}) in order to ensure a complete conversion of nickel oxide into metallic nickel. After this pretreatment step, the temperature was decreased to 200 °C and the test of dry reforming of methane was started. This was conducted under atmospheric pressure, using a reactants ratio CH_4/CO_2 of 1:1 (each reactant being diluted at 10% in Ar) with a total flow of 120 mL min^{-1} (Gas Hourly Space Velocity (GHSV) =144 L g^{-1} h^{-1}). The activity of the catalyst was measured by first increasing the temperature from 200 °C up to 650 °C (5 °C min^{-1}), then maintaining the temperature at 650 °C for 12 h for stability measurements. The gaseous products were analyzed online by an Agilent 490 micro-GC equipped with Plot-U (for the detection of CO_2) and molecular sieves (for the detection of H_2, CH_4, and CO) channels and a thermal conductivity detector (TCD) (See details for the calculations in Supp. Inf. section).

Details on the preparation of additional samples (Ni^{II}/S) as well as on the characterization methods for the fresh and spent catalysts can be found in the supporting information section.

3. Results and discussion

In a first step, the respective amounts of nickel(II) nitrate, ammonium carbonate, HEA16Br and distilled water were varied in order to get the formulation of an optimized colloidal suspension ($Ni^{II}_{aq.coll}$) with 0.4 mM of nickel and the following HEA16Br/Ni = 1.7 and $(NH_4)_2CO_3$/Ni = 2.3 molar ratio. The examination of $Ni^{II}_{aq.coll}$ by transmission electron microscopy (TEM) (Fig. 1) revealed nanoparticles of nickel species with a narrow size distribution centered at *c.a.* 1 nm. A complementary Dynamic Light Scattering (DLS) experiment confirmed that the mean hydrodynamic diameter of the particles was lower than 5 nm. The role of HEA16Br could also be clearly emphasized since, in its absence, the mixture of $Ni(NO_3)_2.6H_2O$ and $(NH_4)_2CO_3$ precipitates immediately. In order to check that the particles present in $Ni^{II}_{aq.coll}$ seen by TEM images (Fig. 1) were not formed by the reduction of Ni(II) under the electron beam of the microscope, an analogous aqueous mixture of $Ni(NO_3)_2.6H_2O$ with HEA16Br (no ammonium carbonate added) was prepared and also examined. TEM images (Fig. S1) issued from this blank experiment were significantly different from those of $Ni^{II}_{aq.coll}$, thus validating, unambiguously, the formation of the nickel(II) colloidal species (Fig. 1) before TEM analysis.

In parallel, reference organic suspensions of Ni(0) particles with either 2 or 5 nm nanoparticles ($Ni^{0}_{org.coll(2)}$ and $Ni^{0}_{org.coll(5)}$, see Fig. S2 and Fig. S3, respectively) were prepared following the protocol described in ref [13].

Figure 1

3.1 Characterization of the Ni-based heterogeneous catalysts derived from colloids

The suspension named $Ni^{II}_{aq.coll}$ was tested as a new nickel(II) precursor for the impregnation of SBA-15 (S) [20] leading, after calcination, to $Ni^{II}_{aq.coll}$/S. The presence of nickel hydroxycarbonate before calcination was revealed on the Differential Thermal Analysis profile of the intermediate solid (Fig. S4, curve B) by an additional weight loss at 450 °C related to the decomposition of the carbonate [21]. It is noteworthy that this loss was not detected when analyzing the material recovered from the impregnation of the SBA-15 support by a mixture of $(NH_4)_2CO_3$ and HEA16Br in the absence of nickel precursor (Fig. S4, curve A). The $Ni^{II}_{aq.coll}$/S solid was compared to $Ni^{II}_{org.coll(2)}$/S and $Ni^{II}_{org.coll(5)}$/S prepared in the same manner from $Ni^{0}_{org.coll(2)}$ and $Ni^{0}_{org.coll(5)}$ (Ni^{II} due to the calcination step). The nickel loading

targeted in all cases was 5 wt.%. After calcination under air at 550 °C during 2 h, all the samples were characterized by TEM and X-ray diffraction (XRD) (Fig. 2 and Fig. S5 A and B).

Figure 2

The detection of nickel particles was quite difficult for $Ni^{II}_{aq.coll}$/S and $Ni^{II}_{org.coll(5)}$/S samples (Fig. 2 and Fig. S5B). No external aggregates could be identified thus indicating that the particles, if they still exist, are well-dispersed. In the case of $Ni^{II}_{aq.coll}$/S (Fig. 2), branch-like structures typical of phyllosilicates could be observed on the periphery of the SBA-15 grains. Indeed, the X-ray diffractogram of $Ni^{II}_{aq.coll}$/S exhibited, in addition to the broad signal centered at about $2\theta = 22°$ assigned to amorphous silica, three broad XRD peaks at $2\theta = 34.1°$, 36.7° and 60.5° corresponding to the (200), (202) and (060) diffraction plans of a nickel phyllosilicate structure (JCPDS no. 49-1859) [22]. We assume that the formation of these Ni phyllosilicates may have been induced by the basicity (pH = 8-9) of the $Ni^{II}_{aq.coll}$ suspension prepared in the presence of ammonium carbonate. No XRD peaks corresponding to NiO could be observed neither for $Ni^{II}_{aq.coll}$/S (Fig. 2), nor $Ni^{II}_{org.coll(5)}$/ (Fig S5 B). On the contrary, aggregates of face-centered cubic NiO nanoparticles (Fm-3m) could be easily identified by XRD and TEM in the case of $Ni^{II}_{org.coll(2)}$/S (Fig. S5 A). In the latter case, the mean crystallite size of NiO was estimated to 13 nm using the Debye Scherrer equation. The evolution of the size of the nanoparticles upon calcination for $Ni^{II}_{org.coll(2)}$/S and $Ni^{II}_{org.coll(5)}$/S samples prepared starting from the organic colloids is in agreement with the well-known higher reactivity of the smaller nanoparticles that leads to more aggregation. A similar trend was observed after the deposition of $Ni^{0}_{org.coll(2)}$ and $Ni^{0}_{org.coll(5)}$ on a mesocellular silica foam (MCF) whose pores are more favorable to aggregation than those of SBA-15. Indeed, TEM analyses (Fig. S6 A and B) clearly reveal that, compared to the 5 nm colloids, the 2 nm ones are definitively unstable upon calcination affording $Ni^{II}_{org.coll(2)}$/MCF materials (Fig. S6 A) with larger nanoparticles than $Ni^{II}_{org.coll(5)}$/MCF (Fig. S6 B). Those results were confirmed by XRD analyses (Fig. S6 A and B) which emphasized nanoparticles of 12 nm for $Ni^{II}_{org.coll(2)}$/MCF instead of 7 nm for $Ni^{II}_{org.coll(5)}$/MCF estimated from the Debye Scherrer equation. It is also noteworthy that, due to a less efficient confinement, the NiO particles in $Ni^{II}_{org.coll(5)}$/MCF were larger than those in $Ni^{II}_{org.coll(5)}$/S.

Despite their small nominal size, aqueous Ni(II) hydroxycarbonate colloids, in $Ni^{II}_{aq.coll}/S$, were less prone to aggregation which leads, after reduction, to a final material, $Ni^{0}_{aq.coll}/S$, with a better metal dispersion [23]. The reducibility of the nickel species in calcined $Ni^{II}_{aq.coll}/S$ and $Ni^{II}_{org.coll(5)}/S$ samples was evaluated using TPR experiments (Fig. S7). The TPR reduction profiles were compared to that of a reference material (Ni^{II}/S) with 6 nm NiO particles (TEM results shown in Fig. S8) obtained by a modified incipient wetness impregnation of SBA-15 with aqueous nickel(II) nitrate. Ni^{II}/S was characterized by two reduction peaks at 360 °C and 550 °C assigned, in agreement with literature [24-25], to nickel with low and high interaction with the support, respectively. It is noteworthy that nickel in both $Ni^{II}_{aq.coll}/S$ and $Ni^{II}_{org.coll(5)}/S$ samples need higher temperatures (superior to 650 °C) to be totally reduced which implies a better metal-support interaction and relatively small mean particle sizes. The reduction of nickel in $Ni^{II}_{aq.coll}/S$ was even a little bit more difficult due to the presence of Ni phyllosilicates on the starting material [26-29]. The Ni wt. % estimated from the H_2 consumption during the TPR could be estimated to 5.5, 3.1 and 2.8 for Ni^{II}/S, $Ni^{II}_{aq.coll}/S$ and $Ni^{II}_{org.coll(5)}/S$, respectively. As expected, a part of nickel was lost in the filtration for the materials prepared by the impregnation of SBA-15 using colloids ($Ni^{II}_{aq.coll}/S$ and $Ni^{II}_{org.coll(5)}/S$ samples).

Tomography analyses of $Ni^{0}_{aq.coll}/S$ (Fig. 3 and S9) emphasized the preservation of the hexagonal pores structure characteristic of SBA-15 after its impregnation with $Ni^{II}_{aq.coll}$ followed by reduction as well as the conversion of Ni-phyllosilicates present on $Ni^{II}_{aq.coll}/S$ into small and well-dispersed Ni^0 NPs. Small and randomly distributed Ni^0 NPs inside the porosity of SBA-15, with all the pores fully accessible from outside, could be observed which was not visible on the traditional TEM image (Fig. 2) where the phyllosilicates were detected just on the outer SBA-15's surface.

Figure 3

3.2 Catalysis performances

After *in-situ* reduction using H_2 (5% in Ar), $Ni^{II}_{aq.coll}/S$, $Ni^{II}_{org.coll(5)}/S$ and Ni^{II}/S were tested as catalysts precursors in the DRM reaction at 650 °C for 12 h using a GHSV of 144 L g^{-1} h^{-1} (Fig. 4). This temperature is interesting, from a thermodynamic point of view, in order to check the occurrence or not of side reactions which generate $C_{(s)}$. Indeed coke deposition is almost impossible at temperature higher than 750 °C [9].

Figure 4

$Ni^0_{aq.coll}$/S showed the best catalytic performances in terms of activity and stability with approximately 70% CO_2 and CH_4 conversions at t=0 h and still 66% after 12 h (Fig. 4). The worst catalyst of the series was the one with the highest Ni loading, Ni^0/S. Not only Ni^0/S led to a rather low conversion at t = 0 h (51% and 56% for CH_4 and CO_2, respectively) but this catalyst was quickly deactivated after approximately 1 h (around 11% for both CH_4 and CO_2 conversions). On the contrary, the catalytic performances of the material prepared starting from the organic colloids, $Ni^0_{org.coll(5)}$/S, which were the lowest at the beginning (41 and 50 % for CH_4 and CO_2, respectively), remained stable and even increased slowly to achieve ≈ 50% for CH_4 and ≈ 55% for CO_2 conversions after 12 h. Such increase could be due to some further *in-situ* reduction of remaining NiO particles by the H_2 produced by the DRM reaction. It is noteworthy that $Ni^0_{aq.coll}$/S led also to the best selectivity with a H_2:CO ratio close to 1 during 12 h on stream whereas $Ni^0_{org.coll(5)}$/S and Ni^0/S catalysts led to a H_2:CO ratio of ≈ 0.8, probably as the result of the occurrence of the Reverse Water Gas Shift side reaction. Best results with $Ni^0_{aq.coll}$/S can be definitively attributed to the use of nickel(II) hydroxycarbonate colloids and to the formation of intermediate Ni-phyllosilicates [30] after the impregnation and calcinations steps. The Ni^0/S material recovered after the test (Fig. S10 A) was characterized by particles with sizes around 8 nm instead of 6 nm before (from XRD results Fig. S11). Moreover, carbon deposition, at the origin of Ni^0/S deactivation during the stability test, could be emphasized by TG analysis and TEM images (Fig. S12 and Fig S10, weight loss of 3-4% at around 550-680°C which explains, in agreement with the XRD results, the absence of carbon diffraction peaks). However, this low amount of carbon seems to be mainly deposited on the big particles outside the grains causing a deactivation limited to the first 2 h of reaction. These observations corroborate other studies showing that larger nanoparticles have higher tendency to form coke than smaller ones [31]. As a matter of fact, no carbon deposition could be detected at all for $Ni^0_{aq.coll}$/S and $Ni^0_{org.coll(5)}$/S (Fig. S12) whose Ni(0) diffraction patterns (2θ = 45 and 52° corresponding to face-centered cubic Ni(0) (JCPDS 70-1849)) were absent before and after (Fig. S11) the 12 h test and whose TEM images (Fig. S10 B, C and D) showed tinny and highly dispersed Ni^0 nanoparticles.

4. Conclusion

In conclusion, aqueous nickel(II) hydroxycarbonate colloids (≈ 1 nm) have been prepared from $Ni(NO_3)_2.6H_2O$, ammonium carbonate and HEA16Br (stabilizing agent) and used, for the first time, to obtain stable Ni^0/SBA-15 DRM catalysts. More importantly, it has been demonstrated that the supported nickel(II) hydroxycarbonate colloids ($Ni^{II}_{aq.coll}$) better resist toward sintering and aggregation than nickel(0) colloids of similar size (2 nm) prepared in organic medium. Such behavior, which is responsible for the best catalytic performances of $Ni^0_{aq.coll}$/S, has been attributed to the formation of Ni-phyllosilicate intermediates emphasized by TEM and XRD analyses. In addition, the tomographic study showed that Ni^0 particles in $Ni^0_{aq.coll}$/S are mainly incorporated into the pores of the SBA-15 silica thus generating a physical barrier that avoid a massive aggregation. Once they have been deposited on silica, Ni(0) colloids prepared by the reduction of Ni(II) by trioctylphosphine in the presence of oleylamine are handicapped by the much more important amount of organics that have to be removed and probably by some contamination of Ni(0). In comparison with other works [31-32], the preparation method described here, for the stabilization of nickel, is simpler (no need of promoters) and leads to smaller Ni NPs resulting in better catalytic performances. It has also to be noted that, among a lot of studies (more than 100 papers) dealing with Ni/silica catalysts in DRM, very few (see Table S1) used Ni silica-based catalysts working with a GHSV ≥ 144 L g^{-1} h^{-1} [33-35]. Hence, clearly $Ni^0_{aq.coll}$/S can be qualified as one of the best Ni/silica-based catalysts. Moreover, the nickel particles size, after deposition onto the siliceous support and reduction, was the tinniest one detected even compared with solids prepared through the deposition-precipitation method that generates phyllosilicates. Those results highlight the importance of controlling the particles size even in the aqueous hydroxycarbonates before generating phyllosilicates and make this method an original one for nickel(0) particles size control.

Acknowledgments

The authors sincerely acknowledge the ERANETMED EU-FP7 initiative, the national ANR (France), CNRS-L (Lebanon) agencies and the Lebanese University for their financial support through the SOL-CARE (Energy-065) project (JC-EN- ERGY-2014 first call) and the French national project METSA for providing them with access to

the microscope platform of IPCMS in Strasbourg. They also gratefully acknowledge Pr A. Roucoux and Dr A. Nowicki (ENSC Rennes, France) for a gift of HEA16Br.

Conflicts of interest

The authors have no conflicts of interest to declare.

References:

[1] H.M. Swaan, V.C.H. Kroll, G.A. Martin, C. Mirodatos, Deactivation of supported nickel catalysts during the reforming of methane by carbon dioxide, *Catal. Today*, 21 **(1994)** 571-578.

[2] X. E. Verykios, Catalytic dry reforming of natural gas for the production of chemicals and hydrogen, *Hemijska Industrija*, 56 **(2002)** 238-255.

[3] N. Mota, C. Alvarez-Galvan, R.M. Navarro, J.L.G. Fierro, Biogas as a source of renewable syngas production: advances and challenges, *Biofuels*, 2 **(2011)** 325-343.

[4] S. Li, J. Gong, Strategies for improving the performance and stability of Ni-based catalysts for reforming reactions, *Chem. Soc. Rev.*, 43 **(2014)** 7245-7256.

[5] S. Kawi, Y. Kathiraser, J. Ni, U. Oemar, Z. Li, E. Toon Saw, Progress in Synthesis of Highly Active and Stable Nickel-Based Catalysts for Carbon Dioxide Reforming of Methane, *ChemSusChem*, 8 **(2015)** 3556-3575. |

[6] Y. Wang, L. Yao, S. Wang, D. Mao, C. Hu, Low-temperature catalytic CO_2 dry reforming of methane on Ni-based catalysts: A review, *Fuel Processing Technology* (**2018**), 169, 199-206.

[7] G. Zhang, J. Liu, Y. Xu, Y. Sun, A review of CH_4-CO_2 reforming to synthesis gas over Ni-based catalysts in recent years (2010-2017), International Journal of Hydrogen Energy, 43 (**2018**), 15030-15054.

[8] O. Daoura, N. El Hassan, P. Massiani, F. Launay, M. Boutros, Influence of synthesis parameters of mesocellular silica foams doped by nickel on methane reforming by CO_2, *MATEC Web of Conferences*, (**2018**) 171, 03002 https://doi.org/10.1051/matecconf/201817103002 II.

[9] D. Pakhare, J. Spivey, A review of dry (CO_2) reforming of methane over noble metal catalysts, *Chem. Soc. Rev.* 43 (**2017**) 7813-7837.

[10] Y. Zhao, Y. Kand, H. Li, H. Li, CO_2 conversion to synthesis gas *via* DRM on the durable Al_2O_3/Ni/Al_2O_3 sandwich catalyst with high activity and stability, *Green Chem*. 20 (**2018**) 2781-2787.

[11] W. Jang, H. Kim, J. Shim, S. Yoo, K. Jeon, H. Na, Y. Lee, D. Jeong, J. Bae, I. Nah, H. Roh, Key properties of Ni-MgO-CeO_2, Ni-MgO-ZrO_2, and Ni-MgO-Ce(1−*x*)Zr(*x*)O_2 catalysts for the reforming of methane with carbon dioxide, *Green Chem.* 20 ***(2018)*** 1621-1633.

[12] O. Daoura, M. N. Kaydouh, N. El Hassan, P. Massiani, F. Launay, M. Boutros, Mesocellular silica foam-based Ni catalysts for dry reforming of CH_4 (by CO_2), *J. CO_2 Util.* 24 *(***2018**) 112-119.

[13] J. Woo Han, J. Seong Parka, M. Suk Choib, H. Lee, Uncoupling the size and support effects of Ni catalysts for dry reforming of methane, *Appl. Catal. B Environ.* 203 ***(2017)*** *625-632.*

[14] E. S. Lokteva, E. V. Golubina, Metal-support interactions in the design of heterogeneous catalysts for redox processes, *Pure Appl. Chem.* 91 *(***2019**) 609-631.

[15] M. Boutros, A. Denicourt-Nowicki, A. Roucoux, L. Gengembre, P. Beaunier, A. Gédéon, F. Launay, A surfactant-assisted preparation of well dispersed rhodium nanoparticles within the mesopores of AlSBA-15: characterization and use in catalysis, *Chem. Commun*. (**2008)** 2920-2922.

[16] J. Huang, R. Buonsanti, Colloidal nanocrystals as heterogeneous catalysts for electrochemical CO_2 conversion, *Chem. Mater.* 31 (**2019**) 13-25.

[17] A. Roucoux, J. Schulz, H. Patin, Reduced Transition Metal Colloids: A Novel Family of Reusable Catalysts? *Chem. Rev.* 102 (**2002**) 3757-3778.

[18] C.-H. Pelisson, C. Hubert, A. Denicourt-Nowicki, A. Roucoux, From Hydroxyalkylammonium Salts to Protected-Rh(0) Nanoparticles for Catalysis in Water: Comparative Studies of the Polar Heads, *Topics in Catalysis* 56 (**2013**) 1220-1227.

[19] G. Cerichelli, L. Luchetti, G. Mancini, G. Savelli, Cyclization of 2-(3-halopropyloxy)phenoxide ions in functionalized surfactants, *Tetrahedron* 51 (1995) 10281-10288.

[20] D. Zhao, J. Feng, Q. Huo, N. Melosh, G.H. Fredrickson, B.F. Chmelka, G.D. Stucky, Tri- block copolymer syntheses of mesoporous silica with periodic 50 to 300 angstrom pores, *Science* 279 (**1998**) 548-552.

[21] G. L. J. P. da Silva, M. L. C. P. da Silva, T. Caetano, Preparation and Characterization of Hydrous Zirconium Oxide Formed by Homogeneous Precipitation, *Materials Research* 5 (**2002**) 149-153.

[22] Z. Bian, S. Kawi, Preparation, characterization and catalytic application of phyllosilicate: A review, *Catal. Today*, 339 **(2020)** 3-23.

[23] M. V. Sivaiah, S. Petit, M.F. Beaufort, D. Eyidi, J. Barrault, C. Batiot-Dupeyrat, S. Valange, Nickel based catalysts derived from hydrothermally synthesized 1:1 and 2:1 phyllosilicates as precursors for carbon dioxide reforming of methane, *Microp. Mesop. Mater.* 140 (**2011**) 69-80.

[24] S. Das, J. Ashok, Z. Bian, N. Dewangan, M.H. Wai, Y. Du, A. Borgna, K. Hidajat, S. Kawi, Silica-Ceria sandwiched Ni core–shell catalyst for low temperature dry reforming of biogas: Coke resistance and mechanistic insights, *Appl. Catal. B: Env.* 230 (**2018**) 220-236.

[25] Z. Bian, S.Kawi, Sandwich-Like Silica@Ni@Silica Multicore–ShellCatalyst for the Low-Temperature Dry Reforming of Methane: Confinement Effect Against Carbon Formation, ChemCatChem 10 (**2018**) 320-328.

[26] O. Daoura, S. Daher, M.N. Kaydouh, N. El Hassan, P. Massiani, F. Launay, M. Boutros, Influence of the swelling agents of siliceous mesocellular foams on the performances of Ni- based methane dry reforming catalysts, Int. J. Hydrogen. Energ. **2018**, 43, 17205-17215.

[27] Z. Bian, S. Kawi, Highly carbon-resistant Ni–Co/SiO_2 catalysts derived from phyllosilicates for dry reforming of methane, *J. CO_2 Util.* 18 (**2017**) 345-352.

[28] T. Wu, Q. Zhang, W. Cai, P. Zhang, X. Song, Z. Sun, L. Gao, Phyllosilicate evolved hierarchical Ni- and Cu–Ni/SiO_2 nanocomposites for methane dry reforming catalysis, *Appl. Catal. A Gen.* 503 (**2015**) 94-102.

[29] Z. Bian, I. Y. Suryawinata, S. Kawi, Highly carbon resistant multicore-shell catalyst derived from Ni-Mg phyllosilicate nanotubes@silica for dry reforming of methane, *Appl. Catal. B: Env.* 195 (**2016**) 1-8.

[30] I. ul Haq, E. Matijević, K. Akhtar, Preparation and Properties of Uniform Coated Inorganic Colloidal Particles. 11. Nickel and Its Compounds on Manganese Compounds, *Chem. Mater.* 9 (**1997**) 2659-2665.

[31] C. Chen, X. Wang, L. Zhang, X. Zou, W. Ding, X. Lu, Synthesis of mesoporous Ni–La_2O_3/SiO_2 by ploy(ethylene glycol)-assisted sol-gel route as highly efficient catalysts for dry reforming of

methane with a H_2/CO ratio of unity, Catal. Commun. 94 **(2017)** 38-41.

[32] R. Benrabaa, A. Löfberg, J. Guerrero Caballero, E. Bordes-Richard, Annick Rubbens, R. N. Vannier, H. Boukhlouf, A. Barama, Sol–gel synthesis and characterization of silica supported nickel ferrite catalysts for dry reforming of methane, *Catal Commun.* 58 **(2015)** 127-131.

[33] A. Rodriguez-Gomez, R. Pereñiguez, A. Caballero. Nickel Particles Selectively Confined in the Mesoporous Channels of SBA-15 Yielding a Very Stable Catalyst for DRM Reaction, *J. Phys. Chem. B* 122 (**2018**) 500-510.

[34] E. C. Lovell, A. Fuller, J. Scott, R. Amal, Enhancing Ni-SiO_2 catalysts for the carbon dioxide reforming of methane: Reduction-oxidation-reduction pre-treatment, *Appl. Catal. B: Env.* 199 (**2016**) 155-165.

[35] E. C. Lovell, J. Horlyck, J. Scott, R. Amal, Flame spray pyrolysis-designed silica/ceria-zirconia supports for the carbon dioxide reforming of methane, *Appl. Catal. A: Gen.* 546 (**2017**) 47-57.

Figure captions

Figure 1: TEM images and particles size distributions of $Ni^{II}_{aq.coll}$.

Figure 2: TEM images and XRD patterns of calcined $Ni^{II}_{aq.coll}$/S.

Figure 3: Tomography analysis of $Ni^{0}_{aq.coll}$/S (reduced at 650°C during 2 h using H_2 5 vol.% in Ar). A: One of the STEM HAADF images extracted from the tilt series used to reconstruct the volume (with the corresponding STEM BF image, inset) of a representative SBA-15 grain. B and C: Typical slices extracted from the reconstructed 3D volume (image (B), inset) obtained by using the 3D approach of the electron tomography. D: The corresponding 3D model of the SBA15 nanograin obtained by using a data segmentation approach from its reconstructed volume.

Figure 4: CH_4 and CO_2 conversions *vs*. time on stream of selected catalysts at 650°C. Conditions: 50 mg of catalysts, 120 $mL.min^{-1}$ as total flow of CH_4 (10% in Ar) and CO_2 (10% in Ar) (GHSV =144 $L.g^{-1}.h^{-1}$).

Figure 1

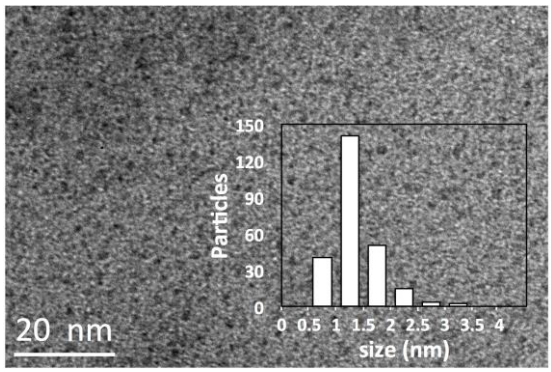

Figure 2

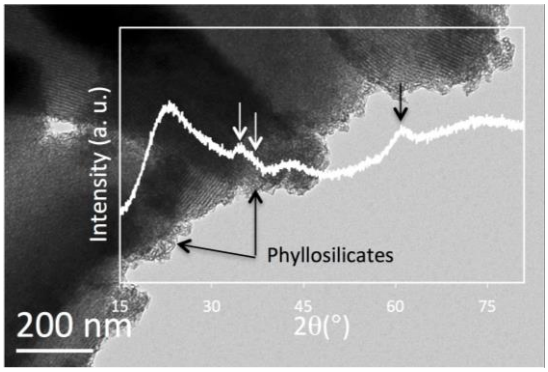

Figure 3

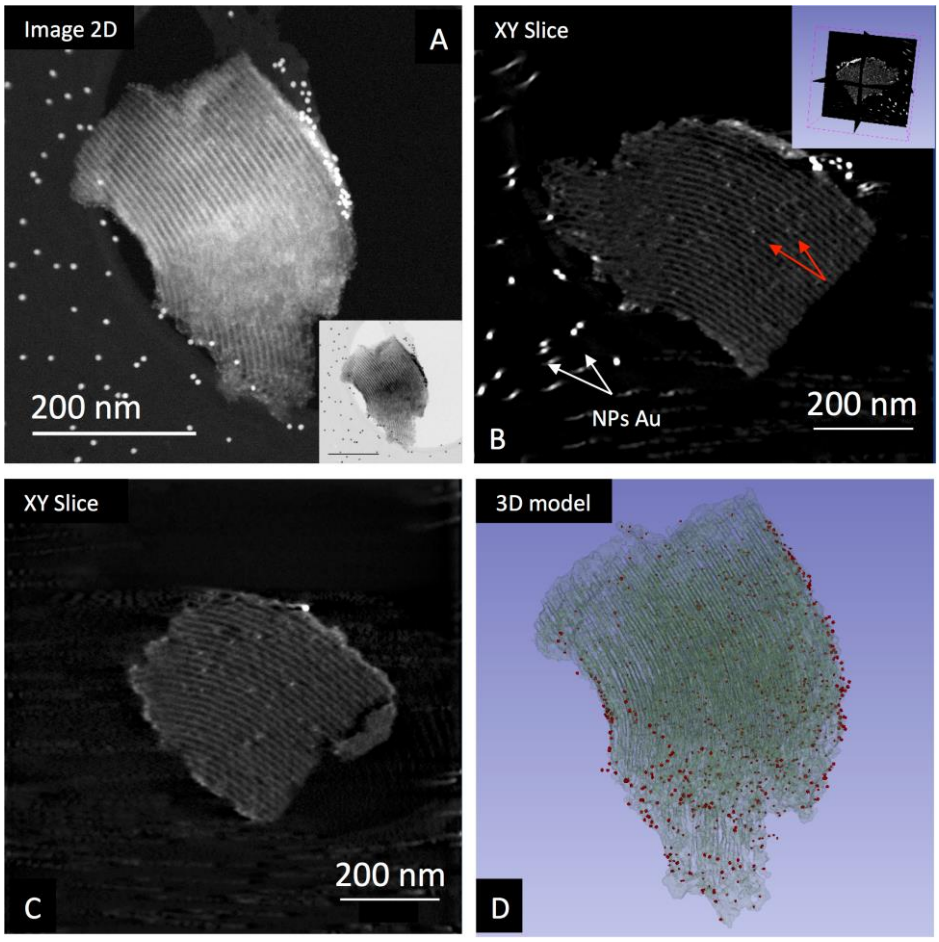

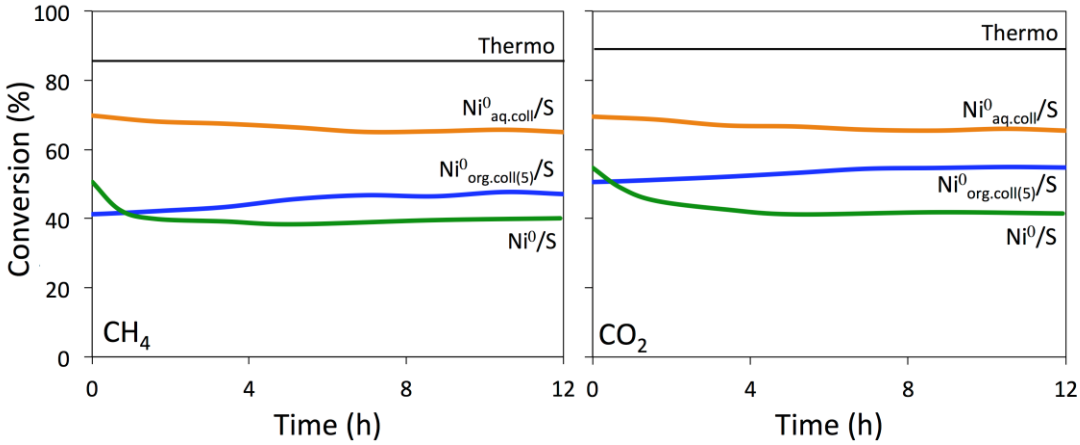
Conversion (%)
100
80
60
40
20
0
Thermo
$Ni^0_{aq.coll}/S$
$Ni^0_{org.coll(5)}/S$
Ni^0/S
CH_4
CO_2
0
4
8
12
Time (h)

Aqueous nickel(II) hydroxycarbonate instead of nickel(0) colloids as precursors of stable Ni-silica based catalysts for the dry reforming of methane

Oscar Daoura[a,b], Ghenwa El Chawich[a,b], Maya Boutros[a], Nissrine El Hassan[c], Pascale Massiani[b], Ovidiu Ersen[d], Walid Baaziz[d], Franck Launay[b*]

[a] Université Libanaise, Laboratoire de Chimie Physique des Matériaux (LCPM/PR2N), Faculté des Sciences II, Campus Fanar, BP 90696 Jdeideh, Lebanon

[b] Sorbonne Université, CNRS, Laboratoire de Réactivité de Surface, LRS, Campus Pierre et Marie Curie, F-75005 Paris, France.

[c] University of Balamand, Faculty Of Engineering, Department of Chemical Engineering, P.O. box 33, Amioun El Koura, Lebanon.

[d] Institut de Physique et de Chimie des Matériaux de Strasbourg (IPCMS), UMR 7504 CNRS - Université de Strasbourg, 23 rue de Loess, BP43, 67034 Strasbourg Cedex 2, France.

Supporting information Section

1. Experimental

1.1 Catalysts preparation

1.1.1 Synthesis of reference "organic" colloids ($Ni^0_{org.coll(2)}$ / $Ni^0_{org.coll(5)}$ suspensions)

The detailed procedure was as follows: Ni acetylacetonate ($Ni(acac)_2$, 1.9 or 0.6 mmol) was mixed with trioctylphosphine (TOP, 19.5 or 4.5 mmol) and oleylamine (OAm, 0 or 24.3 mmol) under vigorous stirring at 215°C or 220°C during 0.5 h or 2 h for $Ni^{II}_{org.coll(5)}$ or $Ni^{II}_{org.coll(2)}$, respectively.

1.1.2 Synthesis of Ni^{II}/S

Another reference catalyst (Ni^{II}/S) was prepared starting from nickel(II) nitrate using the "Two-Solvents" impregnation method. The procedure was as follows:

Commercial SBA-15 (Sigma-Aldrich CAS number: 7631-86-9, 1g) was suspended in 35 mL of cyclohexane, then a volume of water equal to the silica pore volume (as previously determined by N_2 physisorption) and containing the appropriate amount of nickel precursor (0.25 g $Ni(NO_3)_2.6H_2O$) was added dropwise. The resulting solid was dried 3 days at room temperature, then overnight at 60°C. After deposition, the the impregnated sample was calcined under air at 550°C during 2 h in order to get Ni^{II}/S.

1.2 Determination of the catalysis performances

The conversions of methane and carbon dioxide were calculated according to equations 1 and 2, respectively, and the H_2/CO ratios were estimated using equation 3:

$$CH_4 \text{ conversion, } \% = \frac{(CH_{4(in)} - CH_{4(out)})}{CH_{4(in)}} \times 100 \quad \text{(equation 1)}$$

$$CO_2 \text{ conversion, } \% = \frac{(CO_{2(in)} - CO_{2(out)})}{CO_{2(in)}} \times 100 \quad \text{(equation 2)}$$

$$H_2/CO = \frac{H_{2(out)}}{CO_{(out)}} \quad \text{(equation 3)}$$

1.3 Characterization techniques

The hydrodynamic diameters D_H of selected colloids were determined by dynamic light scattering (DLS, Malvern, Zeta Sizer NanoZS instrument). X-ray Diffraction (XRD) data were recorded on a X'Pert3 Powder diffractometer (PANalytical, Netherlands) using CuKα radiation. The average nickel particle size for each sample was calculated from the Scherrer equation: $D=K\lambda/\beta\cos\theta$, where K is a constant (K=0.9), λ=1.5405 Å, β is the full width at half maximum (FWHM) of the diffraction peak and θ is the peak position. Nickel reducibility in the prepared (calcined) materials was studied by Temperature Programmed Reduction (TPR), carried out on an Autochem 2920 (Micromeritics) apparatus equipped with a TCD detector. The samples (80 mg) were heated on a quartz wool in a U-shaped quartz sample tube from room temperature to 800 °C at a rate of 10 °C min^{-1} using a gaseous mixture (25 mL

min^{-1}) of 5 vol% H_2/Ar. An ice and salt bath was used to remove water formed during reduction before the TCD detector. Transmission Electronic Microscopy (TEM) analyses were performed on a JEOL-2010 (LaB6) microscope operating at 200 kV. Before observation, the sample powder was dispersed in ethanol, the resulting suspension was deposited on a copper grid coated with a porous carbon film and the grid was left in ambient atmosphere for ethanol evaporation. The 3D imaging by electron tomography was performed in the scanning transmission electron microscopy (STEM) mode using a JEOL 2100 FEG S/TEM microscope operated at 200 kV and equipped with a probe spherical aberration corrector. The sample was dispersed in ethanol and deposited on a holey carbon coated TEM grid. For the acquisition of the STEM-HAADF (high annular dark field) images, a spot size of 0.13 nm, a current density of 140 pA and a camera length of 8 cm (corresponding to inner and outer diameters of the annular detector of about 73 and 194 mrad), were used. The acquisition of tilt series was acquired using the tomography plug-in of the Digital Micrograph software which controls the specimen tilt step by step, the defocusing and the specimen drift. The spatially correlated HAADF and BF tilt series were acquired by using the ADF and BF detectors and tilting the specimen in the angular range of ± 66° using an increment of 2° in the equal mode, giving thus 65 images in each series. These images were spatially aligned by using a cross correlating algorithm; the volume reconstruction was subsequently calculated using the algebraic reconstruction technique (ART) ot the TomoJ plugin implemented in the ImageJ software. Finally, the visualization and the analysis of the 3D reconstructions were carried out using the displaying capabilities and the isosurface rendering method of the Slicer software. Thermogravimetric analyses (TGA) were performed in order to quantify the carbon deposits on the spent catalysts using a TA SDT Q600 thermal analyzer instrument. Measurements were carried out from RT to 900 °C (heating rate 10 °C.min^{-1}) in flowing air (100 mL min^{-1}). Textural properties were determined from N_2 adsorption-desorption isotherms recorded on an ASAP 2020 (Micromeritics) apparatus. Prior to measurements, the samples were degassed under vacuum for 2 h at 250°C. Specific surface areas were obtained using the BET equation. Pore diameters and specific pore volumes were determined using the BJH model.

2. Figures and tables

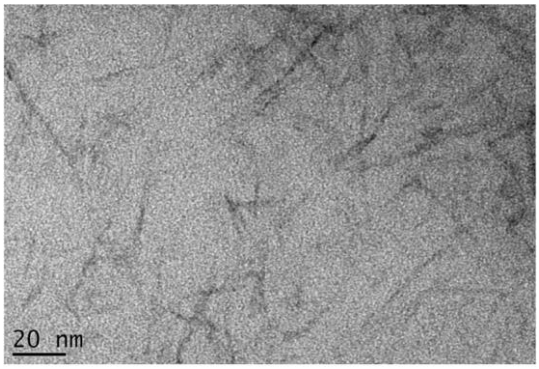

Figure S1: TEM image of a mixture of an aqueous solution of $Ni(NO_3)_2.6H_2O$ and HEA16Br (in the absence of $(NH_4)_2CO_3$).

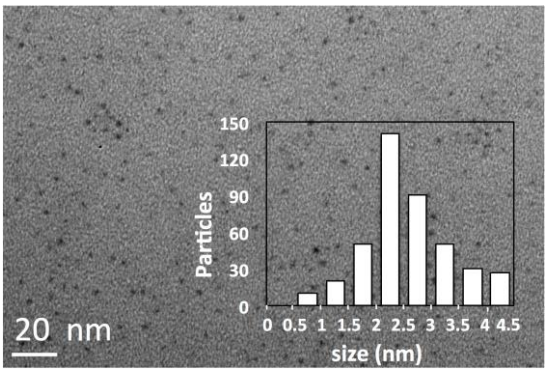

Figure S2: TEM image of $Ni_{org.coll(2)}$ and size distribution histogram.

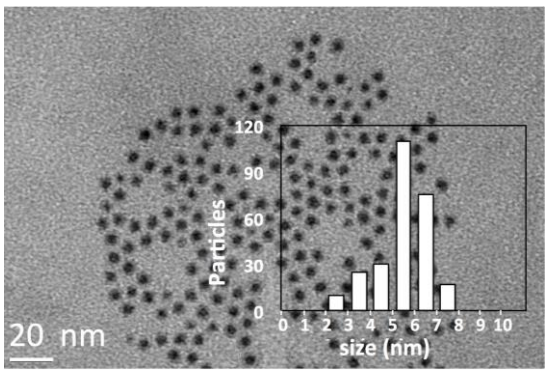

Figure S3: TEM image of $Ni_{org.coll(5)}$ and size distribution histogram.

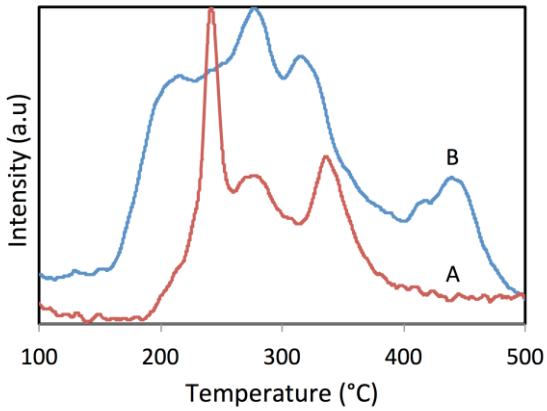

Figure S4: First derivative of the TGA curves for the non-calcined $Ni^{II}_{aq.coll}$/S (blue curve, B) and for a SBA-15 impregnated by a solution of HEA16Br and $(NH_4)_2CO_3$ (red curve, A).

Comments on figure S4:

The weight loss between 150 and 380°C would correspond to the thermal degradation of HEA16Br. Differences between the positions of the derivative maxima for SBA-15 impregnated by a solution of HEA16Br and $(NH_4)_2CO_3$ (Fig. S4, red curve) and for the non-calcined $Ni^{II}_{aq.coll}$/S (Fig. S4, blue curve) would be the consequence of differences in the interaction of HEA16Br with silica (red curve) instead of Ni species (blue curve). However, it is important to note that an additional derivative peak (Fig. S4) between 400 and 480°C was only detected in the case of $Ni^{II}_{aq.coll}$/S before calcination. The latter corresponds to the weight loss due to CO_3^{2-} decomposition (under the form of CO_2 detected from Mass spectroscopy coupled to the TGA).

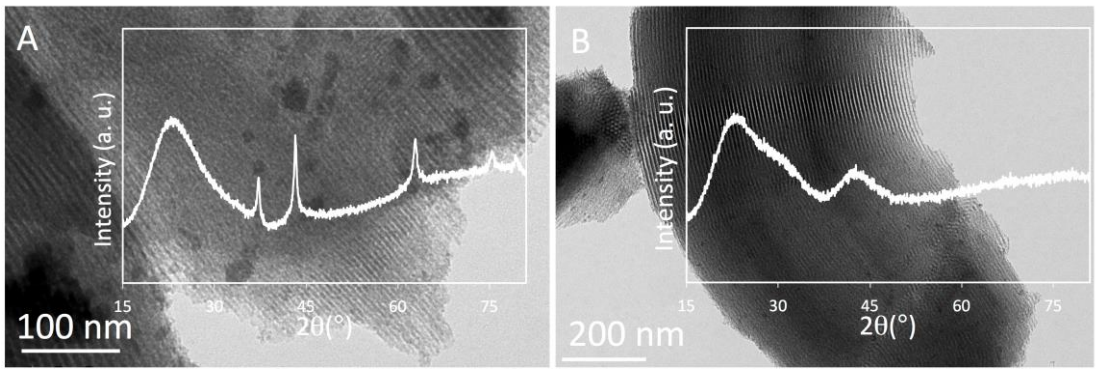

Figure S5: TEM images and XRD patterns of calcined A: $Ni^{II}_{org.coll(2)}$/S and B: $Ni^{II}_{org.coll(5)}$/S.

(For $Ni^{II}_{org.coll(2)}$/S, 2θ = 37, 43, 62, 76 and 80° (JCPDS 89-7130) can be unambiguously assigned to (111), (200), (220), (311) and (222) diffraction peaks of the face-centered cubic lattice (Fm-3m) nickel oxide).

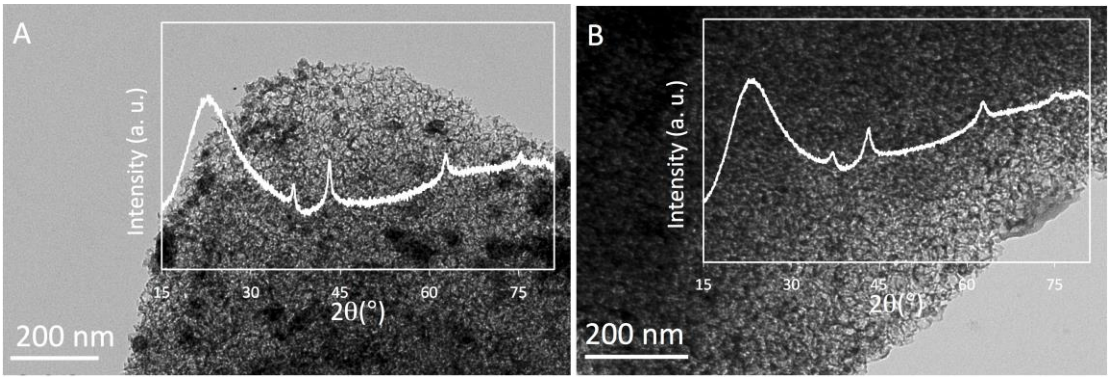

Figure S6: TEM images and XRD patterns of calcined A: $Ni^{II}_{org.coll(2)}$/MCF and B: $Ni^{II}_{org.coll(5)}$/MCF.

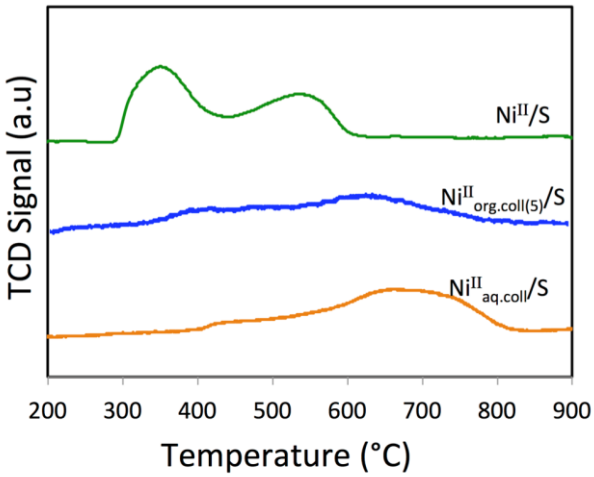

Figure S7: Temperature programmed reduction (TPR) of the calcined solids.

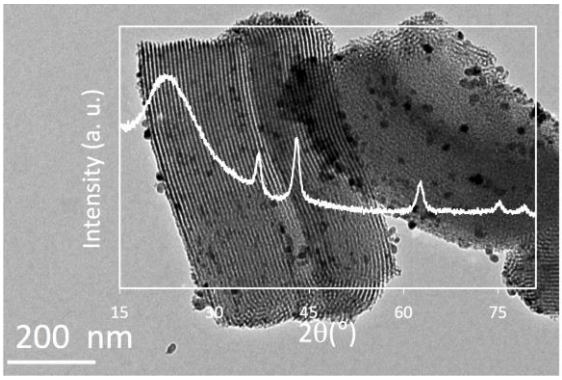

Figure S8: TEM images and XRD patterns of calcined of the Ni^{II}/S sample.

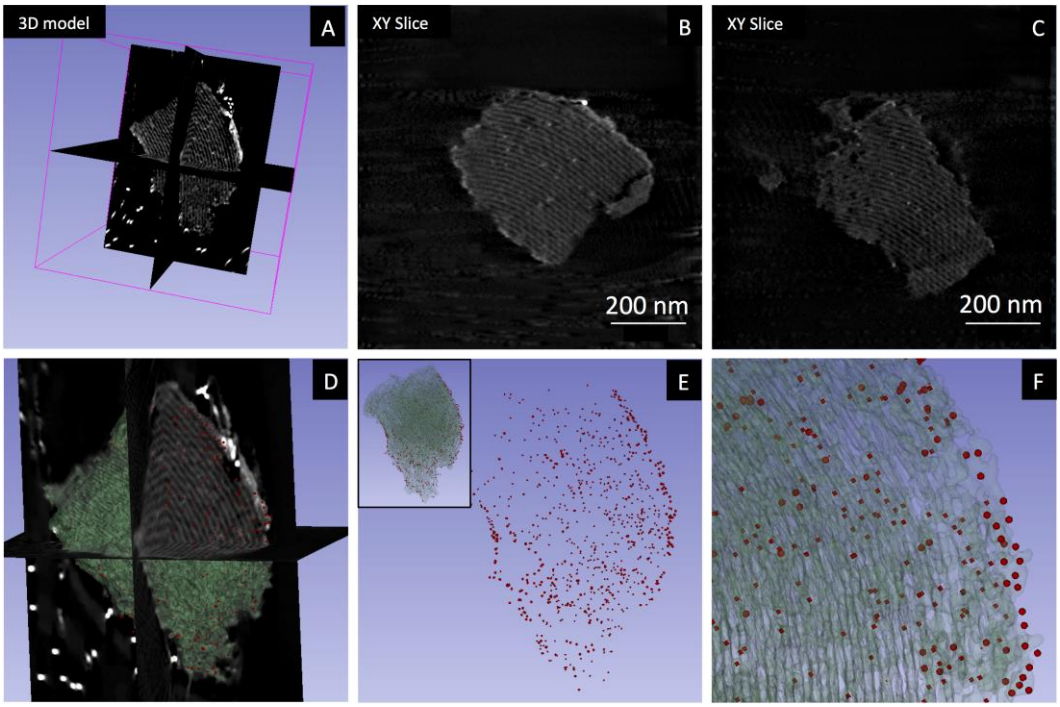

Figure S9: 3D tomography analysis of the $Ni^0_{aq.coll}$/S showing A: the volume calculated for the aggregate shown of the area present in Figure 3 (A), B and C: Typical slices extracted from the 3D volume shown in A), D: Superposed 3D volume and 3D model, E: 3D model of only Ni particles and F: the 3D model of the whole grain (No particles and SBA15 support) showing the presence of small particles inside the SBA15 matrix and bigger ones at the external surface.

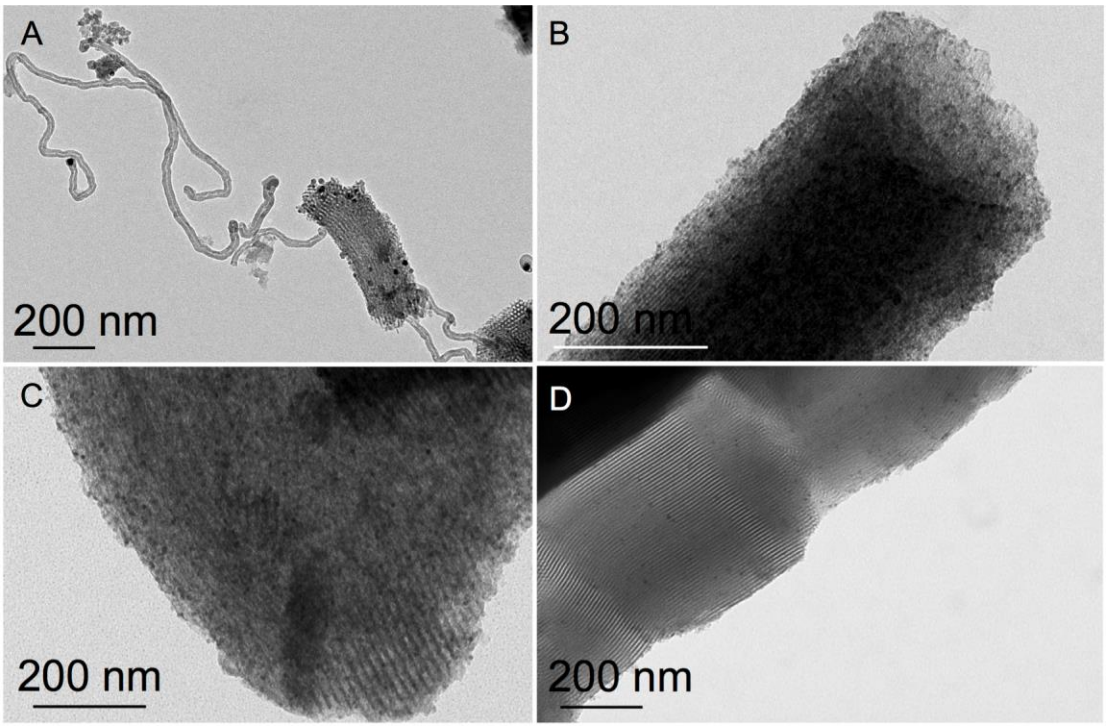

Figure S10: TEM images of spent catalysts A: Ni^0/S, B and C: $Ni^0_{aq.coll}$/S and D: $Ni^0_{org.coll(5)}$/S.

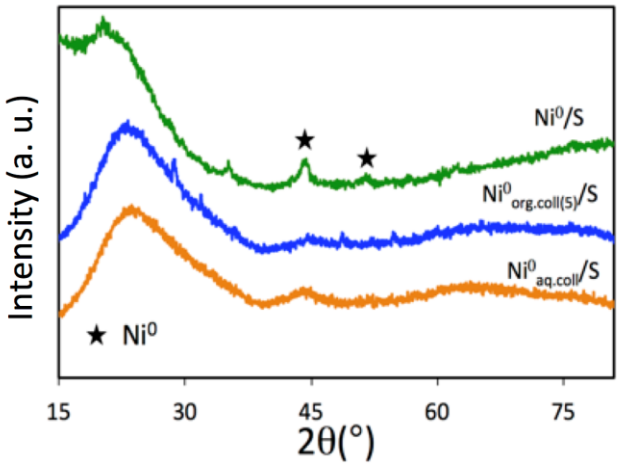

Figure S11: XRD patterns of the spent catalysts.

Comments on figure S11

The small peaks detected in the case of $Ni^0_{org.coll(5)}/S$ and Ni^0/S (other than those corresponding to Ni^0) could be related to the presence of some quartz from the wool used to fix the catalysts inside the reactor [1].

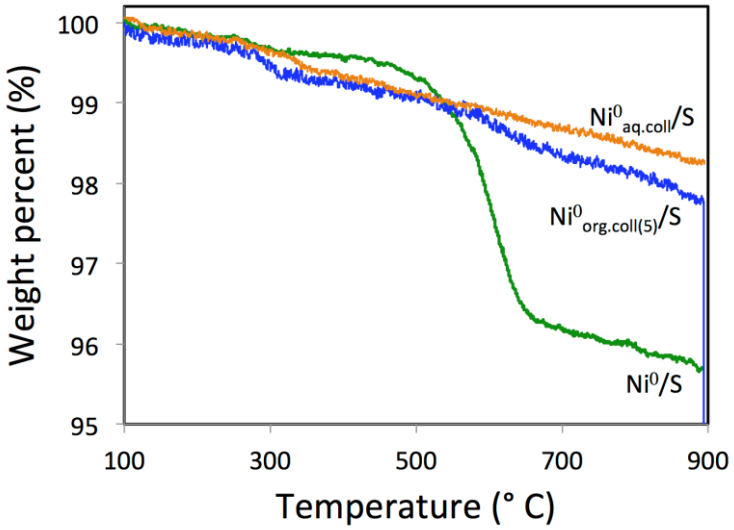

Figure S12: TGA curves of the spent solids ($Ni^0_{aq.coll}/S$, $Ni^0_{org.coll(5)}/S$ and Ni^0/S).

Table S1: Selection of papers published between 2015 and 2018 with GHSV≥ 144 L g^{-1} h^{-1}

Year	Ni (wt.%)	NiO or (Ni^0) size (nm)	Siliceous support	Preparation method	GHSV L g^{-1} h^{-1}	T [a] (°C)	Time [b] (h)	CH_4 [c] %	CO_2 [d] %	Ref
2018	10	5.7 (3.7)	SBA-15, M. SiO_2	IWI + ultrasound D.P	240	750	35	60	n.d.	[2]
2016	5, 10	4	N.P. SiO_2	WI	144	600	12	6	n.d.	[3]
2017	10	5.3	N.P SiO_2	WI	144	700	24	50	n.d.	[4]
	3	(1-2)	SBA-15	WI	144	650	12	66	66	This work

[a]: Temperature of the stability test; [b]: Time of the stability test; [c]: conversion of CH_4 by the end of the stability test; [d]: conversion of CH_4 by the end of the stability test; M.: Mesoporous; N.P.: Non-Porous; TS: "Two-solvents"; WI: wet impregnation; D.P: deposition-precipitation; n. d. : Not determined.

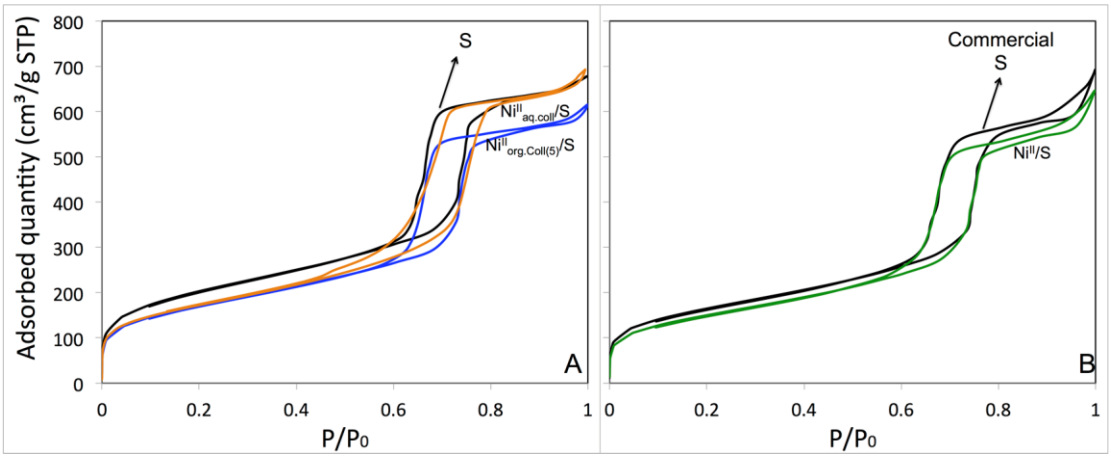

Figure S13: N_2 adsorption-desorption isotherms at -196 °C of the calcined solids.

Table S2: Textural properties of the calcined solids.

Sample	S_{BET} ($m^2.g^{-1}$)	V_{pores}[a] ($cm^3.g^{-1}$)	D_{pores}[b] (nm)
S	674	1	6
$Ni^{II}_{org.Coll(5)}$/S	580	0.8	6
$Ni^{II}_{aq.Coll}$/S	614	1	6
Commercial S	593	1	7
Ni^{II}/S	543	1	6

[a] Total pore volume estimated from BJH desorption

[b] Average pores diameter deduced from BJH desorption pore size distribution

Comments on figure S13 and table S2

Before impregnation, both synthesized and commercial SBA-15 (S) showed type IV isotherms with a H1 hysteresis loop typical of mesoporous materials.

After impregnation by Ni^0 organic colloids (5 nm), the shape of the isotherms was maintained. Therefore, a small decrease in the textural properties especially in the specific surface area and the pores volume was observed which is in good line with the TEM results (Fig. S5B). On the other hand, the $Ni^{II}_{aq.coll}$/S sample showed slightly tilted isotherms. This behavior can be explained by some attack of the silica that can be attributed to i) the basic character of the $Ni^{II}_{aq.coll}$ aqueous suspension used for the impregnation and ii) the formation of Ni phyllosilicates detected by TEM and XRD (Fig. 2).

After impregnation of the commercial silica using the "Two-solvents" method, the shapes of the isotherms were also retained (Ni^{II}/S) and a small decrease in the textural properties could be emphasized.

References

[1] Y. Ruan, Z. Zhang, H. Luo, C. Xiao, F. Zhou, R. Chi, Effects of Metal Ions on the Flotation of Apatite, Dolomite and Quartz, *Minerals 8 (***2018**) 141-153.

[2] A. Rodriguez-Gomez, R. Pereñiguez, A. Caballero. Nickel Particles Selectively Confined in the Mesoporous Channels of SBA-15 Yielding a Very Stable Catalyst for DRM Reaction, *J. Phys. Chem. B 122 (***2018**) 500-510.

[3] E. C. Lovell, A. Fuller, J. Scott, R. Amal, Enhancing Ni-SiO_2 catalysts for the carbon dioxide reforming of methane: Reduction-oxidation-reduction pre-treatment, *Appl. Catal. B: Env. 199 (**2016**)* 155-165.

[4] E. C. Lovell, J. Horlyck, J. Scott, R. Amal, Flame spray pyrolysis-designed silica/ceria-zirconia supports for the carbon dioxide reforming of methane, *Appl. Catal. A: Gen. 546 (***2017**) 47-57.